Geochemical Journal, Vol. 49, pp. 413 to 419, 2015 doi:10.2343/geochemj.2.0365

Geochemical characteristics of absorbed gases in fault gouge from the Daliushu dam area, NW China

XIANGXIAN MA,[1] GUODONG ZHENG,[1]* SHOUYUN LIANG[1,2] and WANG XU[1,3]

[1]Key Laboratory of Petroleum Resources, Gansu Province/Key Laboratory of Petroleum Resources Research, Institute of Geology and Geophysics, Chinese Academy of Sciences, Lanzhou 730000, P.R. China
[2]Key Laboratory of Mechanics on Disaster and Environment in Western China (Lanzhou University), Ministry of Education, Lanzhou 730000, P.R. China
[3]Graduate University of Chinese Academy of Sciences, Beijing 100029, P.R. China

(*Received August 19, 2013; Accepted April 7, 2015*)

A total of eleven fault gouge samples were collected from the Daliushu Dam area in the Zhongwei-Tongxin Fault Zone (ZTFZ) and analyzed for the absorbed gas geochemistry. The concentration of absorbed gas was between 0.04 and 1.65 cm^3STP/g, and the chemicals were determined as mainly CO_2, N_2, H_2, Ar, and a few hydrocarbon gases. The ratios of N_2 and Ar suggest the presence of water in the fault zone, leading to water-rock interaction and lower N_2/Ar ratios. CO_2 and H_2 showed some signatures implying abiogenic origin, with relatively high $\delta^{13}C_{CO2}$ (–1.7‰ to 0.95‰) and H_2 being positively correlated to CO_2 ($r = 0.83$). We speculate that the CO_2 and H_2 are correlated to lithic origins in the fault zone, carbonate and silicate, respectively. On the other hand, CH_4 did show a biogenic signature, with low $\delta^{13}C_{CH4}$ (–44.2‰ to –45.6‰). The variation trends among the absorbed gases in the fault profile show that the gas concentration is mainly related to the fault zone structure, petrology of the fault material, and porosity. The total amounts of absorbed gases including H_2, CO_2, and Ar observed were higher at site F201 than those at site F3, and since the F201 site is known to be much more active than F3, we propose that CO_2, H_2, and Ar could be useful indicators of fault activity.

Keywords: fault gouge, absorbed gas, geochemical characteristics, fault activity

INTRODUCTION

There are several large-scale and important tectonic faults located in the northeast edge of the Qinghai-Tibet Plateau, including the Zhongwei-Tongxin and Haiyuan fault zones. These fault zones are seismically very active, with numerous major earthquakes recorded in human history, such as the Ms 7.5 Zhongwei Earthquake in Zhongwei County in 1709 and the Ms 8.5 Haiyuan Earthquake in Haiyuan County in 1920 (Han, 2004). Each caused severe damage to human society. At present, several large construction projects have been carried out and/or are planned in this region (for example, the Ding-Wu highway, the Baotou-Lanzhou railway, the petroleum pipe from western to eastern China, and the Daliushu Dam) and all are located in parallel with, or crossing, the Zhongwei-Tongxin Fault Zone (ZTFZ). Since seismic activity from these faults may cause significant damage to these projects, it is essential to study the geological properties of these fault zones. Gas geochemistry has previously been used for this because the fault fractures and porosity permit geological fluid and deep gas migration, which may reveal significant information on the properties and kinetics within the faults (Annunziatellis *et al.*, 2008; Ioannis and Dimitris, 2009), even pointing out the locations of particular intense fault activity (Wang *et al.*, 1991).

Gases in fault zones often show significant difference in chemical speciation and relative concentrations. Some, such as radon and helium, have even been proposed to be effective earthquake predictors, (e.g., Bräuer *et al.*, 2003; Stephen *et al.*, 2004; Fu *et al.*, 2005, 2008) and indicators of concealed faults (e.g., Ciotoli *et al.*, 1999; Walia *et al.*, 2013) because these gases are mainly derived from the deep Earth and transferred to the surface through active fault zones. Although many reports describe soil gases in fault zones (e.g., Ciotoli *et al.*, 1998; Karsten, 2008; Zhou *et al.*, 2010; Walia *et al.*, 2010), only a few are focused on the spatial distribution of absorbed gas patterns within the context of certain fault zone profiles, in order to probe the relationship between these gases and fault activity (e.g., Lewicki *et al.*, 2003; Mahajan *et al.*, 2010). In this study, we investigate the distribution and geochemical characteristics of absorbed gases in fault

*Corresponding author (e-mail: gdzhbj@mail.iggcas.ac.cn)

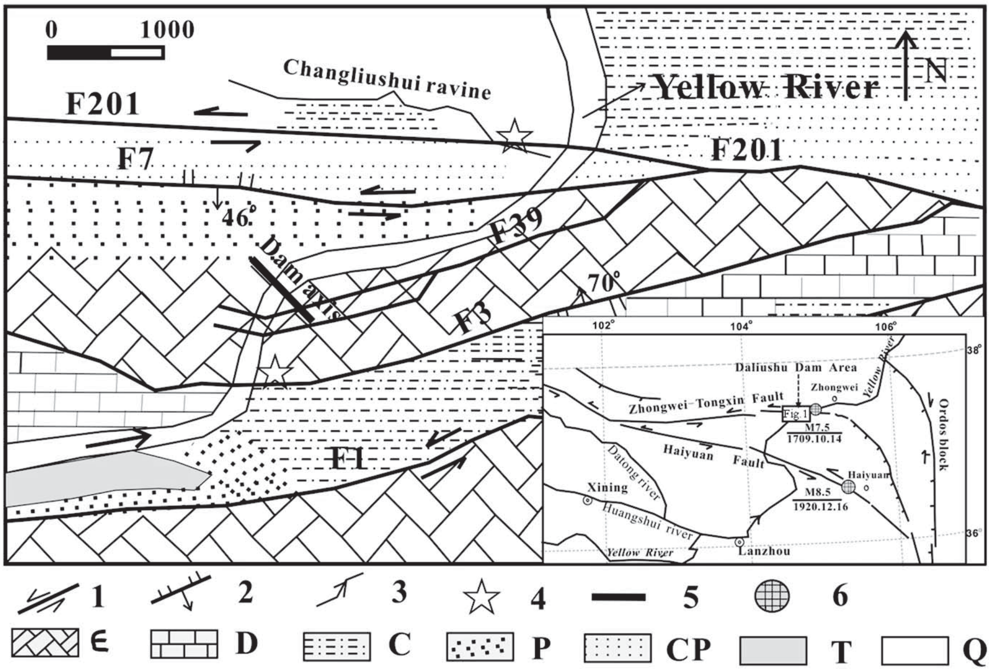

Fig. 1. Geological map of the Daliushu area (simplified after Guo et al. (2004) and Han (2004)). 1 slip fault, 2 reverse fault, 3 rivers, 4 sampling points, 5 the planned dam axis, and 6 earthquake location. Є: the Cambrian system; D: the Devonian system, C: the Carboniferous system; P: the Permian system; CP: the Carboniferous-Permian systems; T: the Triassic system; Q: the Quaternary system.

gouges within the Daliushu Dam area, and then discuss their significance with regard to the fault zone features and activity.

Geological Setting

The Daliushu Dam area, located in Gansu Province, northwest China, is a key area in that part of the Yellow River using dams. It is also a significant tectonic region located along the northeast edge of the Qinghai-Tibet Plateau (Chu, 2009), where many large-scale faults have developed, mainly including F201 and F3 (Guo *et al.*, 2004). F201 is the backbone fault of the ZTFZ, and is the seismogenic fault of the Ms 7.5 Zhongwei Earthquake in 1709. F201 has a strike angle of 290° and a dip angle of 45° to 70°. The surface rupture of this fault zone is approximately 110 km long and 10 to 35 m wide. The F201 fault has mainly developed through Cambrian and Carboniferous strata and cuts through Holocene strata (Han, 2004). The Carboniferous strata overthrusts the Holocene strata in the sampling location, indicating that the last activity of the F201 fault occurred after the Holocene period.

The F3 fault borders the southern part of Daliushu Dam. F3 has a strike angle of 60°, a dip angle of 45°, a trace length of 13 km, and width of 100 m. The Cambrian strata overthrusts the Carboniferous strata at the sampling location. The last activity of F3 occurred before the Pleistocene and after the Carboniferous (Han, 2004; Liang *et al.*, 2006). It is an old thrust fault (Han, 2004).

The stratum in the study area consists mainly of Cambrian, Carboniferous, and Quaternary systems. Greenish gray quartzite arkose with a phylliteis is common within the Cambrian strata while the Carboniferous and Quarternary strata primarily contain black silty shale.

Samples and Experiments

The faults F201 and F3 were selected for this study mainly because they are the border faults of the Daliushu Dam, and thus are relevant for the security of the dam. Second-order faults around the dam axis also formed part of this study (Fig. 1). Study samples were collected perpendicular to F201 (site-F201), where the Changliushui river joins the Yellow river, at the point where a newly unearthed section crosses the fault on a fresh scarp. To avoid cross contamination, nine samples of fault gouge and rocks with different weathered surfaces were stripped and collected from depths between 0.2 and 0.5 m in a vertical, bottom-up profile (GK-03 to GK+06), as shown in Fig. 2. The samples of GK-01, GK-02, and GK-03 were collected from the footwall, while GK+01 to GK+06 were

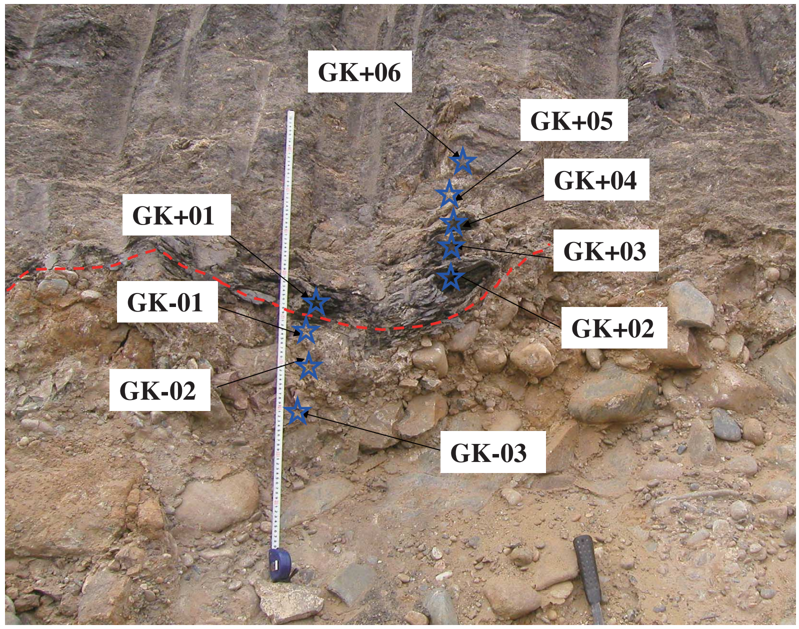

Fig. 2. Photograph showing the outcrop of fault F201 with gouge and sampling points. The dotted line represents the fault plane.

Table 1. Samples for study: Petrological properties and location

Sample ID	Petrological characteristics	Location	Porosity (%)	Host rock
Site-F201				
GK+01	Fault gouge, black mudstone	Upward to fault plane 0–2 cm	1.6	Black silty shale
GK+02	Fault gouge, black mudstone	Upward to fault plane 3–6 cm	2.2	
GK+03	Fault gouge, grayish olive mudstone	Upward to fault plane 7–10 cm	2.8	
GK+04	Fault gouge, black mudstone	Upward to fault plane 16–18 cm	1.2	
GK+05	Fault cataclastic, yellow mudstone	Upward to fault plane 25–30 cm	2.1	Glutenite
GK+06	Fault cataclastic, black mudstone	Upward to fault plane 50–60 cm	3.9	
GK-01	Fault gouge, yellow mudstone	Downward to fault plane 0–3 cm	1.3	Black silty shale
GK-02	Fault cataclastic, yellow mudstone	Downward to fault plane 4–9 cm	4.3	Glutenite
GK-03	Fault cataclastic, yellow siltstone	Downward to fault plane 25–30 cm	5.1	
Site-F3				
BK+01	Fault gouge, black mudstone	Fault zone	1.8	Black silty shale
BK+02	Fault gouge, black mudstone	Fault zone	1.9	

collected from the upper wall. Two samples were collected from F3 (site-F3) near the Daliushu Dam axis, both located on the upper wall near the fault plane. Sample characteristics and locations are shown in Table 1.

Samples were first crushed into powder (about 200 mesh) using an agate mortar and pestle in a clean laboratory. The samples were then placed in an ultrasonic vibrator and cleaned using CH_2Cl_2 solution to remove impurities on the particle surfaces. Finally, the samples were dried at 80°C. Subsequently, 1 g of processed sample was prepared for testing. We then used the heat mass spectrometry method employing a Finnigan MAT 271 mass spectrometer. The prepared samples were placed in a quartz glass tube and then sealed and evacuated for approximately 0.5 h at 1×10^{-4} Pa before sealing. Next, they were grade heated from 0°C to 280°C to ensure that all gases were released. The released gases were passed through a refrigeration system at approximately –60°C to eliminate H_2O and to prevent the chemical reaction of CO_2 and H_2O at high temperatures. Finally, the gases were input to the MAT 271 mass spectrometer for gas composition analysis then sent on to a Thermo Finnegan

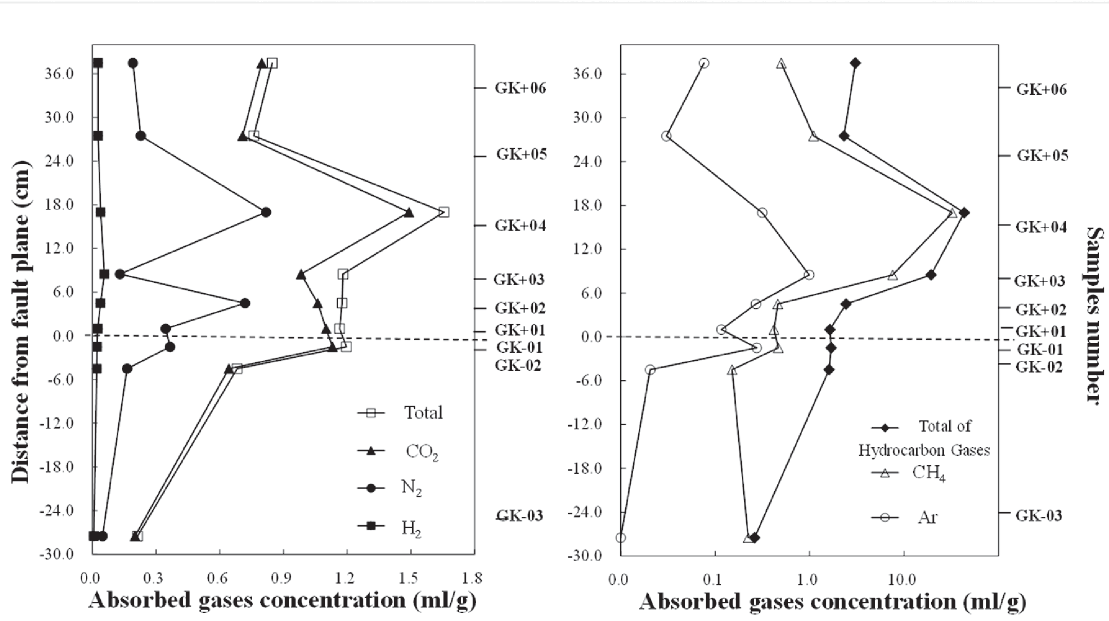

Fig. 3. Variation trends in absorbed gas concentrations at the fault gouge from site-F201 in the vertical profile. Numerical zero represents the fault plane location. Positive and negative values represent upward and downward directions from the fault, respectively.

Deltaplus spectrometer for analysis of their carbon isotope composition (Li *et al*., 1998; Varlam *et al*., 2008).

RESULTS AND DISCUSSION

Composition and origins of absorbed gases

The chemical and isotopic composition of the absorbed gas samples are listed in Table 2. The concentration of absorbed gases is variable in a range from 0.04 to 1.65 cm^3STP/g relative to solid materials or rocks. The fault gouges from F201 and F3 were found to contain mainly carbon dioxide (0.033 to 1.49 cm^3STP/g), with nitrogen (0.00062 to 0.082 cm^3STP/g), hydrogen (0.0019 to 0.039 cm^3STP/g), and a few hydrocarbon gases and noble gases in lesser amounts. Methane (0 to 0.032 cm^3STP/g), ethane (17 to 1590 ppm), and propane (0 to 8710 ppm) were the dominant hydrocarbon gases while argon (5.13 to 315 ppm) was the only noble gas detected (Table 2). Therefore, it seems the fault gouge in the Daliushu area is enriched in absorbed CO_2.

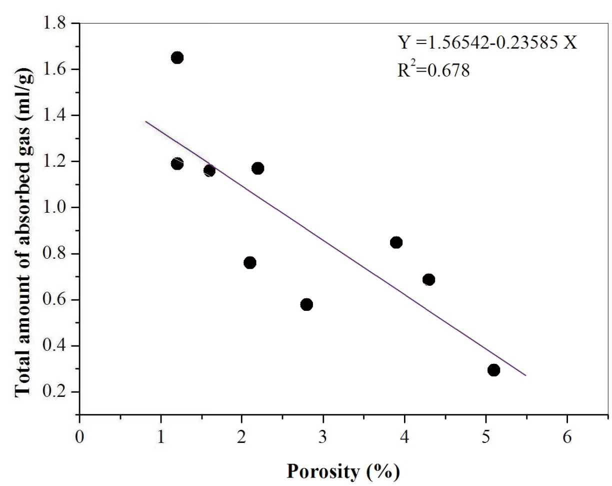

Fig. 4. The relationship between the total amount of absorbed gas and porosity of samples from site-F201.

With the exception of sample GK-01, the ratios of absorbed N_2/Ar were between 7 and 58. The samples GK-03 and BK+02 lay between atmospheric (84) and air-saturated groundwater (ASW = 38.4) the others were in the range between 7 and 38.4. It has been suggested there was a clear negative correlation between the N_2/Ar ratio and water temperature (Xu *et al*., 2012). Such a variation can be explained by the different rates of gas release from individual samples. At very low rates of degassing (low temperature), as may have occurred for GK-03, the composition of gases released from waters originally saturated with air approaches that of air itself, with N_2/Ar ratios approaching the 84 level typical of the atmosphere. At high rates of gas release (high temperature), as may have occurred for GK-06, all the water-dissolved gases get released and N_2/Ar ratios approach those of typical ASW. Since the N_2/Ar ratios of the other samples were lower than that of ASW, we speculate that rock/water interactions were limited in these locations.

Carbon dioxide comprised over 80% of total absorbed gases, ranging from 0.03 to 1.49 cm^3STP/g, with the $\delta^{13}C_{CO2}$ ranging from –1.7‰ to 0.95‰, indicating both biotic and abiotic origins. Xu *et al.* (2012) considered that the $\delta^{13}C_{CO2}$ ratio of CO_2 derived from carbonate thermal decomposition in metamorphic rock was close to that of carbonate rocks, i.e., around 0 ± 3‰, while the $\delta^{13}C_{CO2}$ of magmatic and mantle-derived CO_2 mainly cluster around –6 ± 2‰. The carbon isotope ratios found among the fault samples in this study were also mostly similar to that of carbonate rocks and close to the typical secondary calcite standard value of 0.5‰ (Sugisaki *et al.*, 1983). This may be an indication of newly formed calcite brought on by faulting and water infiltration in the fault zone.

Hydrogen concentration was in a range between 1.85 and 4.86%. There is a positive correlation between H_2 and CO_2 ($r = 0.83$, not shown), suggesting a common origin of the two end members. Moreover, biogenetic hydrogen is always associated with methane production, but the absorbed gases contained little hydrogen gases. Instead, hydrogen atom groups could be liberated from quartz surfaces when they are grinding and crushing during fault movement; such atoms may react with water to produce gaseous H_2 (see Eq. (1)), as shown in laboratory experiments (Sugisaki *et al.*, 1983).

$$3\text{Si}\bullet + H_2O = 3\text{Si-OH} + H\bullet,\ 2H\bullet = H_2. \quad (1)$$

Methane was in the range between 110 and 581 ppm with $\delta^{13}C_{CH4} \approx -44$‰, indicating a biogenetic origin, probably due to microbial action and/or oxidization effects on organic matter.

Absorbed gas variation trend in the vertical profile

In the vertical profile of site-F201, absorbed gases from samples GK+01, GK+02, GK+04, and GK+06 exceeded those of GK-01, GK-02, GK+03, GK-03, and GK+05. The distribution of the absorbed gases follows a pattern. Based on samples taken from the upper wall of the fault, the total amount of absorbed gas increased with the distance from the fault plane. There is an exception in the case of GK+03. It had a grayish olive color indicative of a clay content (5%) half that of the black samples (10%). Its adsorptive capability was likely weaker than the other samples owing to this compositional difference. The total amount of absorbed gases starts to decrease upon nearing the vicinity of the fault gouge-cataclasite boundary. At the footwall and in thin fault gouges, the total amount of absorbed gases decreased with distance from the fault plane, reaching a minimum at the damaged host rock. A similar pattern was evident for the hydrocarbon gases and CO_2 (Fig. 3).

Table 2. Chemical composition of absorbed gases of fault gouge from the Daliushu area

Sample ID	H_2	N_2	O_2	Ar	CO_2	SO_2	CH_4	C_2H_6	C_3H_8	Total	N_2/Ar	$\delta^{13}C_{CO2}$	$\delta^{13}C_{CH4}$
	(cm³STP/g solid)											(PDB, ‰)	
Site-F201													
GK-01	2.20E-2	3.66E-2	3.68E-3	2.75E-4	1.13E+0	1.20E-5	4.66E-4	8.37E-4	3.71E-4	1.19E+0	133	0.50	–44.2
GK-02	2.07E-2	2.08E-2	n.d.	2.05E-5	6.43E-1	n.d.	1.91E-4	1.37E-3	7.50E-5	6.86E-1	30.9		
GK-03	6.93E-3	4.83E-3	n.d.	1.20E-5	2.81E-1	n.d.	2.24E-4	1.70E-5	n.d.	2.93E-1	58.2		
GK+01	2.56E-2	3.45E-2	8.85E-4	1.16E-4	1.10E+0	n.d.	4.19E-4	8.61E-4	3.49E-4	1.16E+0	31.9	–0.75	–44.4
GK+02	3.82E-2	7.19E-2	n.d.	2.70E-4	1.06E+0	1.41E-4	1.75E-3	1.31E-3	4.47E-4	1.17E+0	14.7	–1.20	–45.2
GK+03	2.77E-2	6.37E-2	n.d.	2.37E-4	4.82E-1	n.d.	1.81E-3	1.03E-3	1.64E-3	5.78E-1	7.57	0.95	–44.6
GK+04	3.93E-2	8.18E-2	n.d.	3.15E-4	1.49E+0	4.97E-5	3.23E-2	1.59E-3	8.71E-3	1.65E+0	18.2	–1.70	–45.6
GK+05	2.69E-2	2.28E-2	n.d.	3.04E-5	7.08E-1	n.d.	1.10E-3	5.24E-4	6.61E-4	7.60E-1	31.1		
GK+06	2.68E-2	1.91E-2	n.d.	7.62E-5	7.98E-1	1.69E-5	5.00E-4	2.71E-4	2.19E-3	8.47E-1	41.8		
Site-F3													
BK-01	2.34E-3	6.21E-4	n.d.	5.13E-5	4.82E-2	3.31E-5	5.81E-4	2.18E-3	n.d.	5.40E-2	12.1		
BK-02	1.90E-3	3.40E-3	5.85E-5	7.80E-5	3.25E-2	n.d.	n.d.	1.25E-3	n.d.	3.91E-2	43.6		
Standard samples (percentage composition)													
Air		78.0%	21.0%	0.930%	0.0350%		0.000200%				83.9		
ASW		63.0%	33.6%	1.64%	1.50%		0.000300%				38.4		

Note: n.d. - not detected, ASW - air-saturated groundwater.

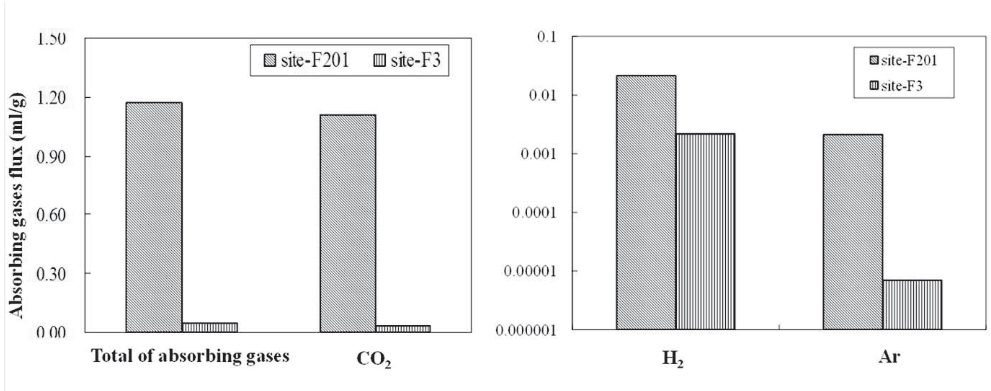

Fig. 5. Differences between the absorbed gas concentrations of the fault gouges from site-F201 and site-F3. The total absorbed gas from site-F201 exceeded that of site-F3, and the main absorbed gas, the total hydrocarbon gases, and noble gases (Ar) all follow the same trend.

The fault zone consists of the fault plane, fault gouge, fault cataclasite, and damaged host rock. The absorbed gas variation trend in the vertical profile was found to be mainly related to the fault material structure and porosity of the fault zone (Fig. 4). In the vicinity of the fault plane, voids were produced during faulting, and gases were released en masse owing to increased porosity. Accordingly, lower amounts of gas could be absorbed in the nearby gouge. As the distance from the fault plane increases, so does the clay content in the fault gouge, which may indicate a self-sealing by fine particles within the fault zone (Zheng *et al.*, 2008) and a stronger adsorptive capacity to trap much more gas. The absorbed gas concentrations in this study are likely lowered dramatically at the cataclasite zone because of these changes in porosity and fracture structures.

Relationship between fault activity and absorbed gas concentrations

Table 2 shows that the absorbed gases from the two faults are very different, possibly a reflection of differences in seismic activity. In comparison, the samples GK+01 and GK+02 (from site-F201) and BK+01 and BK+02 (from site-F3) are similar: they are belong to the same lithological formation (black silty shale) as the host rock and they have similar porosity (about 2.0%). All these samples were collected from areas that are nearest to the fault plane so that their location might be best-suited to represent the latest fault activity. However, the absorbing gases in these samples are sharply different from each other.

The average of absorbed gas amount from site-F201 was 0.94 cm^3STP/g, with CO_2, H_2, and Ar levels at 0.89 cm^3STP/g, 0.021 cm^3STP/g, and 148 ppm, respectively. The average of the amount of absorbed gas from site-F3 was 0.047 cm^3STP/g, with CO_2, H_2, and Ar levels at 0.040 cm^3STP/mg, 0.0021 cm^3STP/g, and 6.5 ppm, respectively. Since the absorbed gases in the fault gouge of F201 exceeded those from F3 by an order of magnitude (Fig. 5) we speculate that the higher absorbed gas levels correspond to increased fault activity. This is based on the reasoning that as the fault becomes more active, water and rock interaction becomes more frequent, leading to increases in the amount of the absorbed gases H_2, CO_2, and Ar.

CONCLUSIONS

The absorbed gases within the fault gouge from F201 and F3 in the Daliushu area are dominated by CO_2, N_2, and H_2 that is most likely derived from rock-water interactions in the fault zone. Comparing F201 with F3, it is shown that CO_2, H_2, and Ar could be an indicator for the degree of rock-water interactions and fault activity; the more active the fault, the greater the degree of water-rock interaction and the higher the concentration of absorbed gases in the gouge. Primarily because of the material structure and porosity, the vertical profile of the F201 fault zone shows a trend with concentrations of absorbed gases increasing with distance from the fault plane until reaching the fault gouge-cataclasite boundary whereupon concentrations decrease and reach minimum values at the damaged host rock.

Acknowledgments—We thank Prof. David Hilton of the Scripps Institution of Oceanography, La Jolla, California and Prof. Giuseppe Etiope from National Institute of Geophysics and Volcanology of Italy for constructive suggestions and for linguistic modification of the manuscript, and two anonymous reviewers for their critical suggestions and comments. This study was supported by the National Natural Science Foundation of China (41273112; 41402129), the Key Laboratory of Petroleum Resources, Gansu Province (1309RTSA041).

REFERENCES

Annunziatellis, A., Beaubien, S. E., Bigi, S., Ciotoli, G., Coltella, M. and Lombardi, S. (2008) Gas migration along fault systems and through the Vadose zone in the Latera caldera (central Italy): Implications for CO_2 geological storage. *International Journal of Greenhouse Gas Control* **2**, 353–372.

Bräuer, K., Kaämpf, H., Strauch, G. and Weise, S. M. (2003) Isotopic evidence (^{3}He/^{4}He, $^{13}C_{CO2}$) of fluid triggered intraplate seismicity. *J. Geophys. Res.* **108**, 1–11.

Chu, Q. Z. (2009) Classification of faults in the Zhongwei Fault Zone and its tectonic implication. *Acta Geologica Sinica* **83**, 1221–1232 (in Chinese with English abstract).

Ciotoli, G., Guerra, M., Lombardi, E. and Vittori, E. (1998) Soil gas survey for tracing seismogenic faults: A case study in the Fucino Basin, central Italy. *J. Geophys. Res.* **103**, 23781–23794.

Ciotoli, G., Etiope, G., Guerra, M. and Lombardi, S. (1999) The detection of concealed faults in the Ofanto Basin using the correlation between soil-gas fracture surveys. *Tectonophysics* **301**, 321–332.

Fu, C. C., Yang, T. F., Walia, V. and Cheng, C. H. (2005) Reconnaissance of soil gas composition over the buried fault and fracture zone in southern Taiwan. *Geochem. J.* **39**, 427–439.

Fu, C. C., Yang, T. F., Jane, D., Liu, T. K., Walia, V. and Cheng, H. C. (2008) Variations of helium and radon concentrations in soil gases from an active fault zone in southern Taiwan. *Radiation Measurements* **43**, S348–S352.

Guo, J. J., Du, D. J., Han, W. F., Chai, S. X. and Liang, S. Y. (2004) Activity of faults $F_{7(8)}$ and F_{201} in the Daliushu Dam region, Heishan Gorge of the Yellow River. *Geological Bulletin of China* **23**, 1259–1264 (in Chinese with English abstract).

Han, W. F. (2004) *Study on Major Engineering Geological Problems in Heishan Gorge of the Yellow River*. Science Press, Beijing, pp. 27–74 (in Chinese).

Ioannis, K. K. and Dimitris, P. (2009) Fluid involvement in the active Helike normal Fault, Gulf of Corinth, Greece. *Journal of Structural Geology* **31**, 237–250.

Karsten, P. (2008) On CO_2 fluid flow and heat transfer behavior in the subsurface, following leakage from a geologic storage reservoir. *Environ. Geol.* **54**, 1677–1686.

Lewicki, J. L., Evans, W. C., Hilley, G. E., Sorey, M. L., Rogie, J. and Brantley, S. L. (2003) Shallow soil CO_2 flow along the San Andreas and Calaveras Faults, California. *J. Geophys. Res.* **108**, 2187.

Li, L. W., Wang, X. B. and Zhang, M. J. (1998) Analysis of hydrogen released by heating olivine. *Geochimica* **27**, 514–516 (in Chinese with English abstract).

Liang, S. Y., Chen, W. W., Han, W. F. and Liu, G. (2006) Initial research on the relationship between absorption gases of fault gouge and fault activity. *Journal of Lanzhou University (Natural Sciences)* **42**, 23–26 (in Chinese with English abstract).

Mahajan, S., Walia, V., Bajwa, B. S., Kumar, A., Singh, S., Seth, N., Dhar, H., Gill, G. S. and Yang, T. F. (2010) Soil-gas radon/helium surveys in some neotectonic areas of NW Himalayan foothills, India. *Natural Hazards and Earth System Sciences (NHESS)* **10**, 1221–1227.

Stephen, A. M., Cristiano, C., Lauro, C., Massimo, C., Massimiliano, B. and Boris, J. P. K. (2004) Aftershocks driven by a high-pressure CO_2 source at depth. *Letters to Nature* **427**, 724–727.

Sugisaki, R., Ido, M., Takeda, H., Isobe, Y., Hayashi, Y., Nakamura, N., Satake, H. and Mizutani, Y. (1983) Origin of hydrogen and carbon dioxide in fault gases and its relation to fault activity. *The Journal of Geology* **91**, 239–258.

Varlam, M., Valkiers, S., Berglund, M., Taylor, P., Gonfiantini, R. and Biévre, P. (2008) Absolute isotope amount ratio measurements on gases Part I: Measurements of isotope amount ratios—Basic theory. *Inter. J. Mass Spectrom.* **269**, 78–84.

Walia, V., Lin, S. J., Fu, C. C., Yang, T. F., Hong, W. L., Wen, K. L. and Chen, C. H. (2010) Soil-gas monitoring: A tool for fault delineation studies along Hsinhua Fault (Tainan) Southern Taiwan. *Appl. Geochem.* **25**, 602–607.

Walia, V., Yang, T. F., Lin, S. J., Kumar, A., Fu, C. C., Chiu, J. M., Chang, H. H., Wen, K. L. and Chen, C. H. (2013) Temporal variation of soil gas compositions for earthquake surveillance in Taiwan. *Radiation Measurements* **50**, 154–159.

Wang, H. L., Chen, J. T., Geng, J. and Wang, L. J. (1991) A study on fault activity in and near Shengli Oil Field. *Northwestern Seismological Journal* **13**, 78–84.

Xu, S., Zheng, G. D. and Xu, Y. C. (2012) Helium, argon and carbon isotopic compositions of spring gases in the Hainan Island, Southern China. *Acta Geologica Sinica* **86**, 1515–1523.

Zheng, G. D., Fu, B. H., Takahashi, Y., Miyahara, M., Kuno, A., Matsuo, M. and Miyashita, Y. (2008) Iron speciation in fault gouge from the Ushikubi fault zone central Japan. *Hyperfine Interactions* **186**(1–3), 39–52.

Zhou, X. C., Du, J. G., Chen, Z., Cheng, J. W., Tang, Y., Yang, L. M., Xie, C., Cui, Y. J., Liu, L., Yi, L., Yang, P. X. and Li, Y. (2010) Geochemistry of soil gas in the seismic fault zone produced by the Wenchuan Ms 8.0 Earthquake, southwestern China. *Geochemical Transactions* **11**, 1–10.